

# Light scattering from cells: the contribution of the nucleus and the effects of proliferative status

J. R. Mourant  
M. Canpolat  
C. Brocker  
O. Esponda-Ramos  
T. M. Johnson  
A. Matanock  
K. Stetter  
J. P. Freyer

Los Alamos National Laboratory  
MS E535  
Bioscience Division  
Los Alamos, New Mexico 87545

**Abstract.** As part of our ongoing efforts to understand the fundamental nature of light scattering from cells and tissues, we present data on elastic light scattering from isolated mammalian tumor cells and nuclei. The contribution of scattering from internal structures and in particular from the nuclei was compared to scattering from whole cells. Roughly 55% of the elastic light scattering at high-angles ( $>40^\circ$ ) comes from intracellular structures. An upper limit of 40% on the fractional contribution of nuclei to scattering from cells in tissue was determined. Using cell suspensions isolated from monolayer cultures at different stages of growth, we have also found that scattering at angles greater than about  $110^\circ$  was correlated with the DNA content of the cells. Based on model calculations and the relative size difference of nuclei from cells in different stages of growth, we argue that this difference in scattering results from changes in the internal structures of the nucleus. This interpretation is consistent with our estimate of  $0.2 \mu\text{m}$  as the mean size of the scattering centers in cells. Additionally, we find that while scattering from the nucleus accounts for a majority of internal scattering, a significant portion must result from scattering off of cytoplasmic structures such as mitochondria. © 2000 Society of Photo-Optical Instrumentation Engineers. [S1083-3668(00)00202-1]

Keywords: optical pathology, tissue diagnostics, DNA content, cancer, cell cycle analysis

Paper JBO-42008 received Sep. 3, 1999; revised manuscript received Dec. 17, 1999; accepted for publication Dec. 22, 1999.

## 1 Introduction

One of the fundamental interactions of light with tissue is elastic light scattering. Measurements of light transport through tissue are consequently sensitive to the structural features of tissue. Since it is these structural features that pathologists often use for disease diagnoses, measurement of light transport through tissue can potentially be a diagnostic tool. A noninvasive optical technique for tissue biopsy and pathology could have several advantages over conventional pathology methods. For example, information can be obtained in real-time, making immediate treatment possible. Additionally, complications and sedatives associated with tissue removal can be eliminated.

There are several noninvasive optical techniques under development. Some methods, such as fluorescence and vibrational spectroscopies, primarily probe biochemical aspects of tissue.<sup>1–3</sup> Other techniques, such as elastic scattering spectroscopy and optical coherence tomography (OCT), measure quantities directly related to light scattering.<sup>4,5</sup> In elastic-scattering spectroscopy broad band light is typically incident on the tissue through an optical fiber. Light that has passed through the tissue is then collected by an adjacent optical fiber and the spectral intensities are measured. The wavelength dependent spectrum of the tissue contains information about both the biochemical and morphological features of the tissue. Optical coherence tomography is an imaging technique in which the intensity of backscattered light from different locations within the tissue is measured at a resolution of  $\sim 10 \mu\text{m}$ . The results described in this paper are most relevant to elastic-

scattering spectroscopy and OCT, but also have relevance to the other optical techniques because all measurements of light transport in tissue are affected by light scattering.

The development of noninvasive optical methods requires a fundamental understanding of how light scatters from structures within tissue. Relevant questions include the following. From what structures does light scatter? How sensitive is light scattering to changes in structural features? Can we quantitate changes in specific structural features from measurements of light scattering? Several research groups have begun addressing these questions. In earlier work, we demonstrated that the average effective radius of the scattering centers in a suspension of fibroblast cells is roughly  $0.2 \mu\text{m}$ , and that there is a wide distribution of sizes with some scatterers being at least  $1 \mu\text{m}$  in radius.<sup>6</sup> Therefore, much of the scattering must be from small structures within the nuclei and cytoplasmic organelles. Mitochondria have been suggested as a major source of scattering, particularly in cells containing a large fraction of mitochondria,<sup>7</sup> and chemically induced megamitochondria have been shown to alter the light scattering properties of cells.<sup>8</sup> Phase contrast microscopy reveals that cell membranes and nuclei cause significant phase shifts compared to other cell components and they are therefore expected to be a major source of light scattering.<sup>9</sup> Theoretical computations of light scattering from cells have elucidated some interesting facts regarding the contribution of nuclei. When nuclei are modeled as a homogeneous structure, high angle scattering is not sig-

nificantly altered as nuclear size is increased. However, when the nucleus is assumed to be heterogeneous, high-angle scattering increases with nuclear size.<sup>10</sup>

The general goal of this work is to examine light scattering from mammalian cells and nuclei using experimental methods. More specifically, light scattering processes related to the interface of the cell membrane with the surrounding media are investigated. The contribution of the nuclei to scattering from whole cells is also determined. Finally, evidence is presented that light scattering from both isolated nuclei and cells is correlated with DNA content, and the possibility that these changes in light scattering are due to changes in nuclear morphology is discussed.

## 2 Methods

### 2.1 Angular Dependent Light Scattering Measurements

Measurements of angular dependent scattering were made as described earlier.<sup>6</sup> Briefly, a HeNe laser was incident on the solution of cells or nuclei. The angular dependent light scattering intensity was measured from 6° to 173° using a photomultiplier tube that was rotated around the sample. (An angle of 180° is defined as backscattering and 0° means no change in the direction of light propagation.) When a concentration of cells between  $1 \times 10^5$  and  $2 \times 10^5$  cells/mL was used, there was at most one scattering event over the pathlength of the sample cell. For a few of the measurements, a higher concentration of cells was used in order to overcome the background scattering from the media. By measuring different dilutions, it was determined that the effect of multiple scattering was negligible between about 30° and 150°. Nuclei were measured at a concentration of  $5 \times 10^5$  nuclei/mL. Because of the lower cross section of scattering from nuclei, there was at most one scattering event over the pathlength of the sample cell.

### 2.2 Elastic-Scatter Spectra of Cell Suspensions

Cells were suspended at a concentration of  $1 \times 10^8$  cells/mL in an open 15 mL volume (depth=3 cm, length=3 cm, width=1.9 cm) sample cell. The container was black on the inside in order to minimize edge effects. Measurements were made with a fiber optic probe placed on the surface of the cell suspension. The optical instrumentation was described in an earlier publication.<sup>11</sup> For these measurements the optical fibers were 200  $\mu\text{m}$  in diameter, the center-to-center separation was 550  $\mu\text{m}$  and all fibers had a numerical aperture of 0.22.

### 2.3 Calculation of Scattering from Spheres

The Mie theory was used to calculate the scattering coefficient of spheres, and the angular dependence of scattering from spheres. The code of Bohren and Huffman<sup>12</sup> was modified in order to calculate scattering from a distribution of sphere sizes. When modeling nuclei, they were assumed to be spherical in shape. The radius was taken to be  $\sim 4.5 \mu\text{m}$  as determined by image analysis. A standard deviation in radius of 2.2  $\mu\text{m}$  was used based on Coulter counter analysis of the nuclear volume distribution. A value of 1.39 was used for the index of the nuclei<sup>13</sup> and a measured value of 1.332 for phosphate buffered saline (PBS) was used for the medium index.

### 2.4 Cell Growth

The highly tumorigenic rat fibroblast cell clone MR1 used in this study was derived from myc-transfected Fisher 344 rat embryo fibroblasts by transfection with the point-mutated T24Ha-ras-oncogene.<sup>14</sup> Monolayer cultures were routinely maintained and subcultured for up to 20 passages (cumulative population doublings 120) as described in detail elsewhere.<sup>15</sup> Briefly, cells were cultured as monolayers in standard tissue culture flasks using Dulbecco's modified eagle's medium (DMEM) containing 4.5 g/l D-glucose, 5% (v/v) fetal calf serum, 100 IU/ml penicillin, and 100  $\mu\text{g}/\text{ml}$  streptomycin. Cell suspensions were obtained from monolayer cultures by treatment for 10 min with 0.25% trypsin in a phosphate buffer (pH 7.4) containing 1 mM EDTA and 25 mM HEPES, followed by the addition of complete DMEM. Growth curve experiments showed that monolayers of MR1 cells reached a plateau in growth at  $\sim 6 \times 10^5$  cells/cm<sup>2</sup>. Based on these data, exponentially growing cell suspensions were obtained from monolayer cultures harvested at a cell density of less than  $2 \times 10^5$  cells/cm<sup>2</sup>, while plateau-phase suspensions were obtained from monolayer cultures harvested at greater than  $6 \times 10^5$  cells/cm<sup>2</sup>. The proliferative status of each of these suspensions was confirmed by flow cytometric DNA content analysis as described below. Exponentially growing cells were composed of 45% G<sub>1</sub>-phase cells, 40% S-phase cells and 15% G<sub>2</sub>-phase cells, while plateau-phase cells were 85% G<sub>1</sub> phase, 5% S phase, and 10% G<sub>2</sub> phase.

### 2.5 Counting of Cells and Nuclei and Volume Analysis of Cells

Suspensions of cells and nuclei were counted using an electronic particle counter essentially as described previously.<sup>16</sup> Briefly, an aliquot of the cell or nuclei suspension was diluted in PBS and three counts were taken using an electronic particle counter (Coulter Electronics) equipped with a pulse-height analysis system for collecting a distribution of the particle volumes. Counts were only taken from a region of the volume distribution that excluded small-volume acellular debris. Volume distributions of cells and nuclei were transferred to a personal computer and analyzed using a standard spreadsheet program (Microsoft Excel™). The cell volume distributions were processed to calculate a mean cell volume from the region not containing acellular debris. Mean volumes were also calculated from the nuclei distributions, but these underestimated the true volume of the nuclei as measured by image analysis (see below) by  $\sim 50\%$ , probably due to the presence of electrically conductive pores in the nuclear membrane. However, nuclei volume distributions were used to both separate nuclei from smaller debris for accurate counting, and to estimate the degree of nuclei clumping.

### 2.6 Nuclei Isolation

Two methods of nuclei isolation were used. One method used a sucrose gradient to separate the nuclei from other cell structures obtained upon lysing of the cell membrane. Briefly, a cell suspension was prepared in reticulocyte standard buffer (MgRSB). This suspension was subjected to a shear force using a Dounce tissue homogenizer in order to rupture the cell membranes. The resulting suspension was centrifuged (10 min at 2000 rpm) to pellet the nuclei and unruptured cells.

The pellet was resuspended in 12 mL of MgRSB and 10 mL of concentrated Mannitol-sucrose buffer and centrifuged for 4 min at 2.5 krpm for sedimentation of the nuclei. The nuclei were then resuspended above layered sucrose solutions. Sucrose buffer 1: 0.32 M sucrose, 3mM CaCl<sub>2</sub>, 2 mM Mg acetate, 0.1 mM EDTA, 10 mM TRIS HCl, 1 mM DTT, and 5% NP-40. Sucrose buffer 2: 2 M sucrose, 5 mM Mg acetate, 0.1 mM EDTA, 10 mM TRIS HCl, 0.1 mM DTT. The nuclei and sucrose solutions were then subjected to ultracentrifugation which resulted in the nuclei being retained at the gradient interface and the unruptured cells and cell fragments being pelleted at the bottom of the tube. The nuclei were removed from the sucrose gradient boundary, resuspended in ice-cold PBS, passed 5 times through an 18-gauge needle, and kept on ice until light scatter analysis. One set of experiments was performed with nuclei isolated by the above method.

We switched to a method adapted from a technique originally developed for flow cytometry of isolated nuclei<sup>17</sup> because it is much faster and resulted in fewer problems with nuclei clumping. A cell suspension in DMEM was added at a 1:3 ratio to a lysis buffer containing 0.6% (v/v) of Nonidet P 40 (a nonionic detergent) and 2 mg/mL bovine serum albumin (BSA) in PBS and incubated for 10 min. The cells were then passed once through a 27.5 gauge needle to break up the cell membranes, centrifuged (10 min at 2000 rpm) and resuspended in 50 mL PBS. The larger particles are then allowed to settle for 5–10 min, and the rest of the sample was then passed 5 times through an 18-gauge needle to break up clumps of nuclei. Electronic volume distributions and image analysis (see below) documented that this procedure produced a suspension of isolated nuclei with little residual cytoplasm and less than 15% of the nuclei in clumps, primarily doublets. Nuclei recovery was 80%–100% of the starting cell population. The final nuclei suspension was kept in ice-cold PBS until light scatter analysis.

## 2.7 Image Analysis

Unfixed cells and nuclei were stained with Hoechst 33342, a DNA specific fluorophore and fluorescein isothiocyanate (FITC), a protein specific chromophore. Images were obtained using a fluorescent microscope interfaced to a computer workstation using commercial image analysis software. Filters were set first to image the Hoechst fluorescence, thereby obtaining an image of the nuclei, then changed to image the FITC fluorescence, thereby obtaining an image of the whole cell for the same microscopic field. The images were processed using standard software (NIH Image) to obtain geometric mean diameters from measurements of the major and minor axes of each nucleus/cell. A total of 200–300 measurements were averaged to obtain an estimate of the cell and nuclear size. Size measurements were essentially identical for the nuclei using the two different filter sets, demonstrating that the nuclei isolation procedure produced nuclei with little residual cytoplasm. Images of 10  $\mu\text{m}$  diameter fluorescent polystyrene spheres were collected for each filter set at the same microscopic magnification and processed using the same settings as for the cells and nuclei. All diameter values have been corrected using the diameter calibration obtained from the microspheres measurements.

## 2.8 Cell Cycle Analysis

DNA content flow cytometry was used to characterize the proliferative status of the cells as described in detail elsewhere.<sup>16</sup> Briefly, a suspension of  $1 \times 10^6$  cells in 1 mL of PBS was fixed in 70% ethanol, then washed with phosphate-buffered saline (PBS) and stained with the nucleic acid stain propidium iodide (50  $\mu\text{g}/\text{mL}$ ) in combination with RNase (100  $\mu\text{g}/\text{mL}$ ) to remove cellular RNA and ensure a fluorescence signal proportional to DNA content. DNA content histograms containing 10,000 cells were then collected using a commercial flow cytometer (FACSCalibur™). DNA content histograms were deconvoluted using a commercial software package (Multicycle™) to estimate fractions of cells in the  $G_1$ ,  $S$ , and  $G_2$  phases of the cell cycle. These histograms had a  $G_1$ -phase peak with a coefficient of variation less than 4%, allowing routine cell cycle analysis which can resolve the different phases with a 2%–3% error.

## 2.9 Manipulation of the Media's Refractive Index

The addition of protein to PBS increases its refractive index. Ovalbumin or BSA (3 gm/ml) were added to PBS, mixed and then filtered through 0.4 and 0.2  $\mu\text{m}$  filters to remove undissolved protein. The exact refractive index of the protein solutions was measured based on the principal of minimum deviation.<sup>18</sup>

## 3 Results

### 3.1 Scattering from Internal Cellular Structures

In order to determine how much of the elastic light scattering was from the cell nucleus or other intracellular structures and how much was related to the cell membrane interface with PBS, we made measurements of cells in media with different indices of refraction. The underlying principle of these experiments is that when the index of refraction difference between the scatterer and the surrounding media is reduced, the intensity of scattering will be reduced.<sup>12</sup> Therefore, when the index of refraction of the medium outside a cell is increased so that it is closer to that of the cell, scattering from the interface between the cell membrane and the external medium will be reduced. Scattering from internal cellular structures, however, will not be affected. For the experiments, equal numbers of cells were suspended in either PBS, with a measured refractive index ( $n$ ) of 1.332, or in a protein solution in PBS. Two sets of measurements were performed. In one set scattering from cells suspended in BSA with  $n = 1.345$  were compared to scattering from cells suspended in PBS. In the other set of measurements, scattering from cells in ovalbumin solution with  $n = 1.343$  were compared to scattering from cells suspended in PBS. Analysis of the size distributions of cells in the different media before and after light scatter assay demonstrated that there were no measurable changes in cell size induced by incubation in these protein solutions. Cell counts before and after light scatter measurement showed a decrease in cell number of <5% during the measurement, probably due to cell adherence to the measuring chamber. Results calculated from our angular dependent scattering measurements are shown in Figure 1. The scattered light intensity at small angles (<20°) was significantly greater when the cells are immersed in PBS with a low refractive index

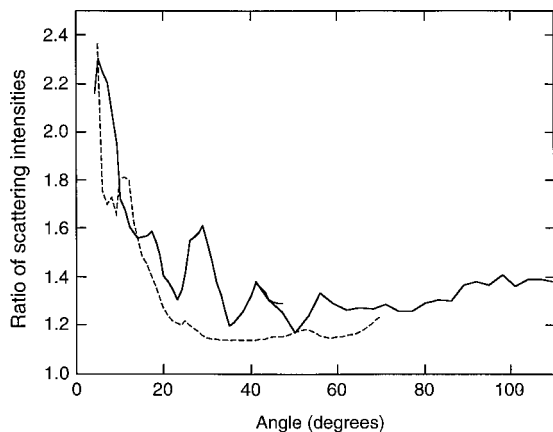


**Fig. 1** Experimentally determined ratio of scattering from cells immersed in media of low and high indices of refraction. The media of low index had a refractive index of 1.332 in both cases. The media of higher index had  $n=1.345$  for the solid curve and  $n=1.343$  for the dashed curve. Data at higher angles are not shown because of interference from scattering off of protein molecules dissolved in the media.

than when they are immersed in a protein solution with a higher refractive index. At larger angles the scattering was not strongly affected by changing to a medium of different index.

In order to learn as much as possible from our experimental results, it was necessary to understand the effects of changing the refractive index of the medium. Consequently, the scattering coefficients of spheres in media of different indices were computed as described in Sec. 2. The ratio of scattering coefficients for spheres immersed in media with indices of 1.330 and 1.345 is plotted as a function of scatterer size in Figure 2. The ratio was only weakly dependent on scatterer size, but it was strongly dependent on the refractive index of the spheres. The closer the refractive index of the spheres was to that of the media, the greater the effect of changing the medium index. The effect of changing the medium refractive index on scattering as a function of angle was also investigated. For scatterers ( $n=1.4$ )  $1 \mu\text{m}$  and smaller in radius, the ratio of light scattering intensity in the medium of lower index

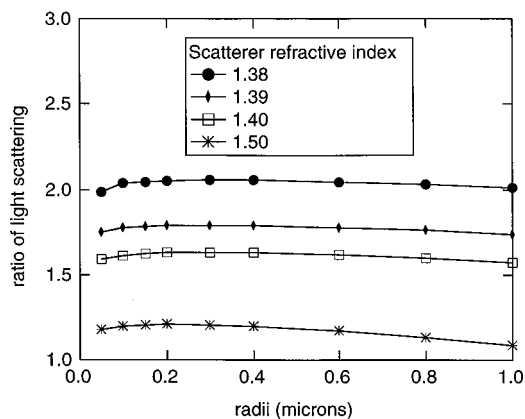


**Fig. 2** Theoretical calculations of the ratio of the scattering coefficients for spheres immersed in media of different refractive indices. The abscissa is sphere size.

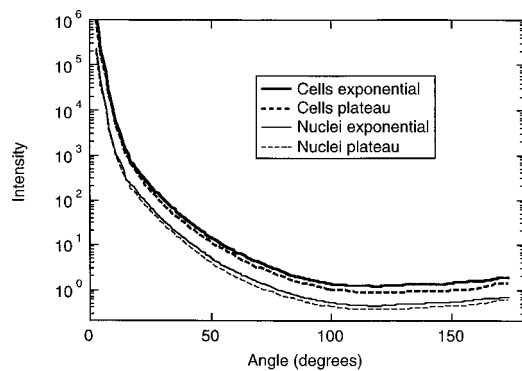
(1.332) to light scattering intensity in the medium of higher index (1.345) did not depend strongly on angle. For larger spheres, the ratio decreased for angles less than about  $15^\circ$ . There were also oscillations as a function of angle for narrow distributions of sphere sizes, but these averaged out when a broader distribution was used. In conclusion, for a distribution of scatterer sizes, scattering at all angles was affected similarly by changing the medium refractive index, with the exception of angles less than about  $15^\circ$ .

We can conclude from the results in Figure 1 that there was significant scattering at small angles from cell structures that are in contact with the medium. However, at larger angles ( $>40^\circ$ ) the effect on elastic scattering of increasing the external index of refraction was much smaller. Assuming a value for the index of refraction of the cell structures in contact with the medium of 1.38 and 1.3 as the ratio of scattering from cells suspended in media with low and high indices of refraction (Figure 1), the fraction of scattering from particles internal to the cell can be estimated from the data at angles above  $40^\circ$ . The scattering in the low refractive index medium is given by  $I_{nc} + I_c$ , where  $I_{nc}$  is the intensity of scattering from structures not in contact with the medium and  $I_c$  is the intensity of scattering from structures in contact with the medium. In the medium of high refractive index, the scattering from the particles in contact with the medium is reduced by about a factor of 2.1 and the scattering is given by  $I_{nc} + 0.48 * I_c$ . Using the fact that the ratio of scattering in the low and high refractive index media is 1.3, we calculate that  $\sim 55\%$  of the elastic light scattering at angles greater than  $40^\circ$  was from internal cellular structures when the cells are immersed in PBS.

### 3.2 Scattering From Cells in the Exponential and Plateau Phases of Growth

The average DNA content of cells harvested in the exponential phase of growth will be different from the average DNA content of cells harvested in the plateau phase of growth, since MR1 cells are known to arrest in the  $G_1$  phase of the cell cycle at growth plateau.<sup>15</sup> Therefore, harvesting cells in different growth stages provides a means of determining whether light scattering is correlated with DNA content. For each experiment, two sets of cells were harvested. In some cases the cells were at similar points on the growth curve, in other cases they were different. Measurements were made of angular dependent light scattering and the DNA content of the cells was determined. In order to quantitate the average DNA content of cells in a population Eq. (1) was used, where  $\%G_2$ ,  $\%S$ , and  $\%G_1$  refer to the percent of cells in the  $G_2$ ,  $S$ , and  $G_1$  phases of the cell cycle, respectively. The basis of Eq. (1) is that cells in the  $G_2$  phase in the cell cycle have two copies of their DNA and therefore have twice as much DNA; cells in the  $S$  phase are in the process of duplicating their DNA and therefore have on average about 1.5 times as much DNA as cells in the  $G_1$  phase of the cell cycle. The fraction of cells in the different stages of the cell cycle were determined by flow cytometric DNA content analysis as described in Sec. 2:

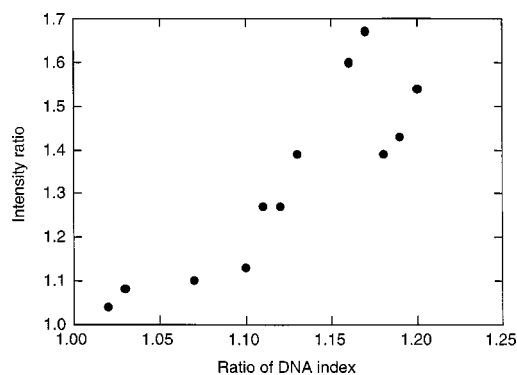
$$\text{DNA index} = 2 * (\%G_2) + 1.5 * (\%S) + (\%G_1). \quad (1)$$



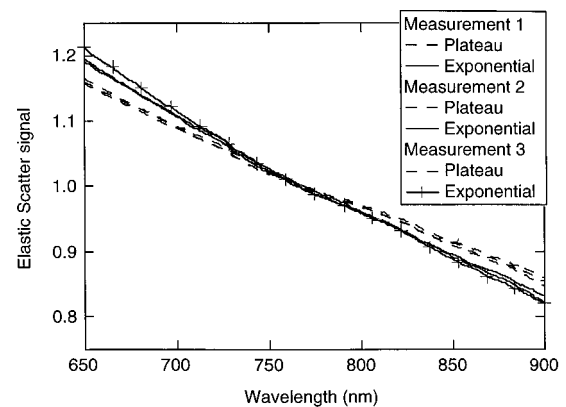
**Fig. 3** Scattered light intensity from cells and nuclei as a function of angle. The curves have been corrected to represent scattering equal number densities of cells and nuclei.

Figure 3 shows representative data from one experiment where the cells were harvested in the exponential and plateau phases of growth. At large angles, the cells harvested in the exponential phase of growth scatter more than those harvested in the plateau phase of growth. To quantify changes in high angle scattering, the integral of the scattering intensity between  $110^\circ$  and  $140^\circ$  was calculated. A ratio of the DNA indices and a ratio of the high angle scattering intensities were computed for each individual experiment. As shown in Figure 4, cell suspensions with larger DNA contents scatter more light than cell suspensions with smaller DNA contents. For example, when one of the suspensions measured contains more DNA than the other, it also has significantly more scattering between  $110^\circ$  and  $140^\circ$ . Clearly, there is a correlation between light scattering at large angles and cellular DNA content.

Elastic scatter spectra of cells in the exponential and plateau phases of growth were also measured. The results for three separate experiments are quite similar, as shown in Figure 5. The slope of the elastic-scatter spectra was steeper for the cells harvested in the exponential phase of growth than for the cells harvested in the plateau phase of growth. Since the wavelength dependence of scattering is generally steeper for



**Fig. 4** Each data point is the result of measurements of two suspensions of cells. In some cases the cells suspensions contained similar amounts of DNA; in other cases one suspension contained significantly more DNA than the other. The ratio of the DNA content of the two suspensions is plotted on the abscissa. The ratio of the scattering intensities from  $110^\circ$  to  $140^\circ$  is plotted on the ordinate.



**Fig. 5** Diffuse reflectance spectra of cell suspensions as a function of wavelength. Results from three separate experiments are shown. The data were normalized such that the area under all of the curves is the same from 650 to 900 nm.

smaller particles,<sup>6</sup> this result indicates that the average size of the scatterers is smaller for the exponential phase cells.

### 3.3 Scattering from Isolated Nuclei

The primary issue we wish to address by examination of isolated nuclei is how much of the scattering from mammalian cells is due to scattering from the nuclei. Nuclei were isolated from cells harvested in the exponential and plateau phases of growth as described in Section 2. Angular dependent scattering measurements were made of cells and the corresponding isolated nuclei. By dividing the results for isolated nuclei by the results for whole cells, we obtained an estimate of the contribution of nuclei to scattering from whole cells.

Figure 3 shows the results of angular dependent scattering measurements from one experiment. As discussed in the above section, cells harvested in the exponential phase of growth scatter more at large angles than cells harvested in the plateau phase of growth. Figure 3 also demonstrates that the nuclei isolated from cells in the exponential phase of growth scatter more at large angles than nuclei isolated in the plateau phase of growth. In Figure 6 we show the ratio of light scattering intensity from nuclei to that from intact cells. For both the exponential and the plateau phase cells, the contribution of the nuclei to the overall scattering from the cells appears to increase with angle. In addition, the contribution of the nuclei appears to be slightly greater for exponential than plateau phase cells. This result held for each of the four individual experiments.

For one of the four experiments (the one in which the nuclei were isolated via the sucrose gradient method), image analysis of the cells and nuclei was performed. The average size of the cells obtained by image analysis was compared to the size obtained by electronic volume analysis. The average diameter of the exponential and plateau phase cells from image analysis was  $14.5$  and  $12.4 \mu\text{m}$ , respectively. The electronic volume results for the two cell suspensions were  $14.6$  and  $12.7 \mu\text{m}$ , respectively, demonstrating that the image analysis technique was accurate. As explained in the Section 2 electronic volume measurements of isolated nuclei were not possible due to the structure of the nuclear membrane. Nuclei

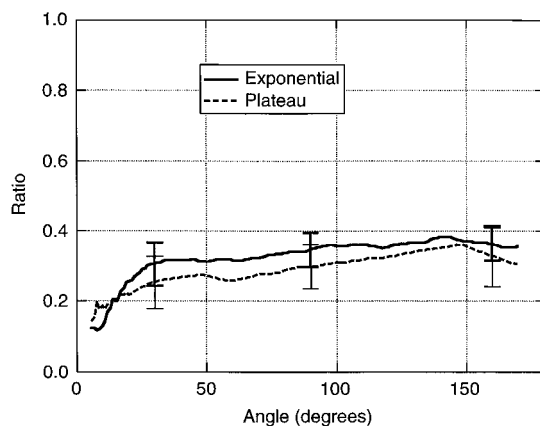


**Fig. 6** Ratio of light scattering from nuclei and cells as a function of angle. The two curves are each the average of four different experiments. Error bars, calculated as the standard deviation of the four measurements, are given for a few points.

isolated from cells harvested in exponential and plateau phases were measured by image analysis and found to have average diameters of  $9.0 \pm 0.18$  and  $9.1 \pm 0.18 \mu\text{m}$ , respectively. The size of the nuclei in intact exponential phase cells was also measured by image analysis and found to be  $8.9 \pm 0.18 \mu\text{m}$ . These results indicate that there is at most a  $0.4 \mu\text{m}$  difference in the average diameter of nuclei harvested in the exponential and plateau phases of growth. To test whether this difference could be responsible for the difference in high angle scattering, model calculations were performed assuming homogeneous nuclei. Nuclei with a diameter of  $9.4 \mu\text{m}$  were found to scatter slightly less at large angles ( $110^\circ$ – $140^\circ$ ) than nuclei with a diameter of  $9.0 \mu\text{m}$ . This difference in scattering, however, is too small to explain the experimental results. The ratio of large angle scattering for the model calculations was only 1.08 compared to the experimentally observed ratio of 1.4 comparing nuclei from exponential- and plateau-phase cells.

#### 4 Discussion

Morphological features have traditionally been used by pathologists to diagnose disease. The exact nature of the sensitivity and specificity of light scattering to morphological changes, however, has not yet been elucidated. The aim of this paper is to contribute to our knowledge of how changes in specific cellular features affect light scattering. In particular we are interested in cellular features that are known to have significance for pathology.

Morphological features of the nucleus such as nuclear size have traditionally been used by pathologists to diagnose malignancy and the relationship of these parameters to optical measurements are being investigated. Perelman et al. have published the results of an analysis of diffuse reflectance measurements for determination of nuclear size assuming homogeneous nuclei.<sup>19</sup> Internal nuclear structures can also be important markers for pathological diagnosis. For example, large nucleoli and clumped chromatin are characteristic of anaplasia.<sup>20</sup> We aimed to directly investigate whether light scattering is sensitive to changes of the internal structure of the nucleus. The same experiment performed with the cells of

comparing scattering when the scatterers were immersed in media of two different indices was attempted. Unfortunately, we found that scattering from the nuclei increased in the ovalbumin solution. Electronic volume measurements indicated that there was no change in nuclear size upon immersion in an ovalbumin solution. Therefore, we attribute this effect to ovalbumin leaking into the nucleus. Nuclear membranes are known to pass proteins of less than 60 kD in molecular weight.<sup>21</sup>

It is possible to obtain insight into light scattering from internal structures of nuclei by combining model calculations and experimental results. Model calculations presented in Sec. 3 as well as those by Drezek et al.<sup>10</sup> demonstrate that a change in size of a homogeneous nuclei cannot be responsible for the increased high angle scattering observed for cells and nuclei harvested in the exponential phase of growth. Additionally, our image analysis results did not show any change in the size of the nuclei. Therefore, we contend that the greater high angle light scattering from nuclei populations with greater DNA content is due to scattering off of internal structures. The elastic-scattering spectra indicate that the average size of the scatterers is smaller in the exponential phase cells. This result is consistent with increased scattering from small structures within the nuclei, although we cannot rule out that this is an effect of structures in the cytoplasm, since cells harvested in the exponential phase of growth are bigger than cells harvested in the plateau phase of growth. We know that exponential-phase MRI cells contain more mitochondria than cells from plateau-phase cultures.<sup>15</sup>

Figure 4 demonstrated that high angle light scattering is sensitive to DNA content. Recently, there has been interest in using DNA ploidy and S-phase fraction for assessing disease status and predicting treatment outcomes.<sup>22–25</sup> For example, DNA ploidy has been shown to be associated with poor outcome for gastric cancer.<sup>25</sup> This raises the issue of whether the elastic-scattering/diffuse-reflectance measurements that are possible in a clinical setting are also sensitive to DNA content. In recent work, we have demonstrated that when elastic scattering is performed with the source and detector in close proximity, the collected light intensity depends on the probability of high angle scattering events.<sup>26</sup> Therefore, we expect that elastic-scattering spectroscopy is sensitive to DNA content. In support of this idea, we have shown in Figure 5 that elastic-scatter measurements of suspensions of cells harvested in different growth phases are reproducibly different.

Our results with cells harvested in different growth phases indicate that scattering from intact cells is probably sensitive to changes in the nuclei. However, the entire difference in scattering of the cells cannot be attributed to only changes in the nuclei. Figure 6 indicates that the nuclei are responsible for less than 40% of the scattering from cells in suspension at any given angle, while Figure 3 and the other angular dependent measurements of scattering from nuclei demonstrates that at most the ratio of scattering from exponential and plateau phase nuclei is 1.5. These numbers predict that the ratio of scattering in exponential and plateau phase cells should be less than 1.2. Figure 4 demonstrates that much larger values are obtained. Therefore, there must be differences in the cell cytoplasm. In fact, we have found that cells harvested in the exponential phase of growth are 1–2  $\mu\text{m}$  larger in diameter than those harvested in the plateau phase of growth, and con-

tain more mitochondria.<sup>15</sup> Further studies are required to elucidate which other intracellular structures contribute to high-angle elastic light scattering.

## 5 Conclusions

High angle light scattering from both cells and isolated nuclei can be correlated with DNA content. The increased scattering of replicating versus nonreplicating cell populations is partly attributed to increased scattering from the nuclei and partly attributed to increased scattering from the cytoplasm. This is consistent with the fact that nuclei were shown to be the source of only about 40% of the scattering from whole cells in suspension.

For this work to be applied clinically, it will be necessary to show that clinical measurements of epithelial tissue are sensitive to replication rate and/or DNA content. As a first step elastic-scatter measurements of suspensions of replicating and nonreplicating cells were made and wavelength-dependent differences were found. We expect our results on cell suspensions to extrapolate to epithelial tissue because it primarily consists of cells. Nonetheless, in epithelial tissue the cells are in direct contact with each other and therefore, the exact nature of the sensitivity of light scattering to DNA content and/or replication rate needs to be elucidated in this situation. In addition, measurement methods that can sensitively and specifically measure scattering properties without interference from absorption need to be developed.

## Acknowledgments

We appreciate the work of David Quintana and Adrienne Stephenson in preparing cells for measurement and for isolation of nuclei. We also acknowledge the assistance of Dr. Stephan Burde and Dr. Babetta Marrone with obtaining and processing images of cells and nuclei. Finally, we acknowledge the assistance of Mona Khalil in collecting and analyzing the flow cytometric DNA content distributions. This work was supported by Grant No. CA-71898 from the National Cancer Institute, Grant No. ES-07845 from the National Institute of Environmental Health Sciences, and Grant No. RR-01315 from the Division of Research Resources, National Institutes of Health.

## References

1. R. Richards-Kortum, and E. Sevick-Muraca, "Quantitative optical spectroscopy for tissue diagnosis," *Annu. Rev. Phys. Chem.* **47**, 555–606 (1996).
2. R. Manoharan, Y. Wang, and M. S. Feld, "Histochemical analysis of biological tissues using Raman spectroscopy," *Spectrochim. Acta A* **52**, 215–249 (1996).
3. M. Diem, S. Boydston-White, and L. Chiroboga, "Infrared spectroscopy of cells and tissues: Shining light onto a novel subject," *Appl. Spectrosc.* **53**, 148A–161A (1999).
4. I. J. Bigio and J. R. Mourant, "Ultraviolet and visible spectroscopies for tissue diagnostics: Fluorescence spectroscopy and elastic-scattering spectroscopy," *Phys. Med. Biol.* **42**, 803–814 (1997).
5. J. G. Fujimoto, B. Bouma, G. J. Tearney, S. A. Boppart, C. Pitris, J. F. Southern, and M. E. Brezinski, "New technology for high-speed and high-resolution optical coherence tomography," *Ann. (N.Y.) Acad. Sci.* **838**, 95–107 (1998).
6. J. R. Mourant, J. P. Freyer, A. H. Hielscher, A. A. Eick, D. Shen, and T. M. Johnson, "Mechanisms of light scattering from biological cells relevant to noninvasive optical tissue diagnostics," *Appl. Opt.* **37**, 3586–3593 (1998).
7. B. Beauvoit, T. Kitai, and B. Chance, "Contribution of the mitochondrial compartment to the optical properties of the rat liver: A theoretical and practical approach" *Biophys. J.* **67**, 2501–2510 (1994).
8. B. Beauvoit and B. Chance, "Time-resolved spectroscopy of mitochondria, cells and tissues under normal and pathological conditions," *Mol. Cell. Biochem.* **184**, 445–455 (1998).
9. J. Beuthan, O. Minet, J. Helfmann, M. Herrig, and G. Muller, "The spatial variation of the refractive index in biological cells," *Phys. Med. Biol.* **96**, 369–382 (1996).
10. R. Drezek, A. Dunn, and R. Richards-Kortum, "Light scattering from cells: Finite-difference time-domain simulations and goniometric measurements," *Appl. Opt.* **38**, 3651–3663 (1999).
11. T. M. Johnson and J. R. Mourant, "Polarized wavelength-dependent measurements of turbid media," *Opt. Express* **4**, 200–216 (1999).
12. C. F. Bohren and D. R. Huffman, *Absorption and Scattering of Light by Small Particles*, Wiley-Interscience, New York (1983).
13. A. Brunsting and P. F. Mullaney, "Differential light scattering from spherical mammalian cells," *Biophys. J.* **14**, 493–453 (1974).
14. L. A. Kunz-Schughart, A. Simm, and W. Mueller-Klieser, "Oncogene-associated transformation of early passage rodent fibroblasts is accompanied by large morphologic and metabolic alterations," *Oncol. Rep.* **2**, 651–661 (1995).
15. L. A. Kunz-Schughart, R. C. Habbersett, and J. P. Freyer, "Mitochondrial function in oncogene-transfected rat fibroblasts isolated from multicellular spheroids," *Am. J. Physiol.* **273**, C1487–C1495 (1997).
16. J. P. Freyer, "Rates of oxygen consumption for proliferating and quiescent cells isolated from multicellular tumor spheroids," *Adv. Exp. Med. Biol.* **345**, 355–342 (1994).
17. A. Krishan, "Rapid flow cytofluorometric analysis of mammalian cell cycle by propidium iodide staining," *J. Cell Biol.* **66**, 188–193 (1975).
18. F. A. Jenkins and H. E. White, *Fundamentals of Optics*, pp. 30–32, McGraw-Hill, New York (1976).
19. L. T. Perelman, V. Backman, M. Wallace, G. Zonios, R. Manoharan, A. Nurst, S. Shields, M. Seiler, C. Lima, T. Hamano, I. Itzkan, J. van Dam, and J. M. Crawford, "Observation of periodic fine structure in reflectance from biological tissue: A new technique for measuring nuclear-size distribution," *Phys. Rev. Lett.* **80**, 627–630 (1998).
20. R. S. Cotran, V. Kumar, and S. L. Robbins, *Pathologic Basis of Disease*, Saunders, Philadelphia (1994).
21. H. Lodish, D. Baltimore, A. Berk, S. L. Zipursky, P. Matsudaira, and J. Darnell, *Molecular Cell Biology*, p. 840, Scientific American, New York (1995).
22. F. Collin, A. Chassevent, F. Bonichon, G. Bertrand, P. Terrier, and J.-M. Coindre, "Flow cytometric DNA content analysis of 185 soft tissue neoplasms indicates that s-phase fraction is a prognostic factor for sarcomas," *Cancer (N.Y.)* **79**, 2371–2373 (1997).
23. F. Esteban, D. S. de Vega, R. Garcia, R. Rodriguez, J. Manzanares, A. Almeida, and S. Tamames, "DNA content by flow cytometry in gastric carcinoma: Pathology, ploidy, and prognosis," *Hepatogastroenterology* **46**, 2039–2043 (1999).
24. J. S. Ross, C. E. Sheehan, R. A. Ambros, T. Nazeer, T. A. Jennings, R. P. Kaufman, H. A. G. Rifkin, and B. V. S. Kallakury, "Needle biopsy DNA ploidy status predicts grade shifting in prostate cancer," *Am. J. Surg. Pathol.* **23**, 296–301 (1999).
25. M. Abad, J. Ciudad, M. R. Rincon, I. Silva, J. I. Pazbouza, A. Lopez, A. G. Alonso, A. Bullon, and A. Orfao, "DNA aneuploidy by flow cytometry is an independent prognostic factor in gastric-cancer," *Anal. Cell. Pathol.* **16**, 223–231 (1998).
26. M. Canpolat and J. R. Mourant, "Quantifying the importance of high angle scattering events to light-transport through turbid media measured in a backscattering geometry," *Phys. Med. Biol.* (submitted).